Alma Mater Studiorum Università di Bologna
Archivio istituzionale della ricerca

Antibacterial composite membranes of polycaprolactone/gelatin loaded with zinc oxide nanoparticles for guided tissue regeneration

(Article begins on next page)

03 May 2024

Antibacterial composite membranes of PCL/gelatin loaded with ZnO nanoparticles for guided tissue regeneration.

Authors and affiliations:

Gina Prado-Prone (PhD) e-mail: gpradoprone@gmail.com

[a]Facultad de Odontología, División de Estudios de Posgrado e Investigación, Universidad Nacional Autónoma de México. Circuito exterior s/n, Ciudad Universitaria, 04510, CDMX, México.

Phaedra Silva-Bermudez (PhD) e-mail: phaedrasilva@yahoo.com

[b]Unidad de Ingeniería de Tejidos, Terapia Celular y Medicina Regenerativa; Instituto Nacional de Rehabilitación Luis Guillermo Ibarra Ibarra; Av. México Xochimilco No. 289 Col. Arenal de Guadalupe C.P. 14389, Ciudad de México, México.

Masoomeh Bazzar (PhD) e-mail: m.bazzar@uea.ac.uk

[c]School of Chemistry, University of East Anglia, Norwich, United Kingdom.

[d]Department of Chemistry "G. Ciamician" and National Consortium of Materials Science and Technology (INSTM, Bologna RU), Alma Mater Studiorum - Università di Bologna, 40126 Bologna, Italy.

Maria Letizia Focarete (PhD) e-mail: marialetizia.focarete@unibo.it

[d]

[e]Health Sciences and Technologies- Interdepartmental Center for Industrial Research (HST-ICIR), Alma Mater Studiorum, Università di Bologna, 40064 Ozzano dell'Emilia, Bologna, Italy.

Sandra E. Rodil (PhD) e-mail: srodil@unam.mx

[f]Instituto de Investigaciones en Materiales, Universidad Nacional Autónoma de México; Ciudad Universitaria No. 3000, C.P. 04360, Ciudad de México, México.

Ximena Vidal-Gutiérrez (MSc) e-mail: ximena.v.gtz@gmail.com

[a]

Jorge A. García-Macedo (PhD) e-mail: gamaj@fisica.unam.mx

[g]Departamento de Estado Sólido, Instituto de Física, Universidad Nacional Autónoma de México; Ciudad Universitaria No. 3000, C.P. 04360, Ciudad de México, México.

Victor I. García-Pérez (PhD) e-mail: victorirahuen@comunidad.unam.mx

[a]

Cristina Velasquillo (PhD) e-mail: m.velasquillo@inr.gob.mx

[h]Laboratorio de Biotecnología, Instituto Nacional de Rehabilitación Luis Guillermo Ibarra Ibarra; Av. México Xochimilco No. 289 Col. Arenal de Guadalupe C.P. 14389, Ciudad de México, México.

Argelia Almaguer-Flores (PhD) e-mail: aalmaguer@comunidad.unam.mx

[a]

Corresponding author: **Argelia Almaguer-Flores**

Mailing address: Facultad de Odontología, División de Estudios de Posgrado e Investigación, Universidad Nacional Autónoma de México. Circuito exterior s/n, Ciudad Universitaria, CP 04510, CDMX, México.

Phone number: +52 55 91992911

Competing Interests

The authors declare that no competing interests are present, and there is no conflict of interest.

Abstract

The bacterial colonization of absorbable membranes used for Guided Tissue Regeneration (GTR) as well as their rapid degradation that can cause their rupture, are considered the major reasons of clinical failure. To address this, composite membranes of polycaprolactone (PCL) and gelatin (Gel) loaded with ZnO-NPs (1, 3 and 6 w% relative to PCL content) were fabricated by electrospinning. To fabricate homogeneous fibrillar membranes, acetic acid was used as a sole common solvent to enhance the miscibility of PCL and Gel in the electrospinning solutions. The effects of ZnO-NPs in the physico-chemical, mechanical and *in vitro* biological properties of composite membranes were studied. The composite membranes showed adequate mechanical properties to offer a satisfactory clinical manipulation and an excellent conformability to the defect site while their degradation rate seems to be appropriate to allow successful regeneration of periodontal defect. The presence of ZnO-NPs in the nanocomposite membranes significantly decreased the planktonic and the biofilm growth of the *Staphylococcus aureus* over time. Finally, the viability of human osteoblasts and human gingival fibroblasts exposed to the composite membranes with 1 w% and 3 w% of ZnO-NPs, indicated that those membranes are not expected to negatively influence in the ability of periodontal cells to repopulate the defect site during GTR treatments. The results here obtained suggests that composite membranes of PCL and Gel, loaded with ZnO-NPs have the potential for being used as structurally stable GTR membranes with local antibacterial properties intended for enhancing the clinical treatments.

Keywords: Periodontal membranes, ZnO nanoparticles, polycaprolactone, gelatin, electrospinning, antibacterial properties, biocompatibility.

1. Introduction

Guided Tissue Regeneration (GTR) technique is the most frequently procedure used to regenerate periodontal tissues defects caused by periodontal disease or trauma [1,2]. This surgical technique employs barrier membranes to prevent epithelial tissue growth at the bone defect site and allow periodontal ligament and alveolar bone cells to repopulate the bone defect facilitating its regeneration [1,2]. GTR membranes require being biocompatible, flexible to conform the site defect, and preferably, biodegradable to eliminate the need for removal surgery. Membranes should present suitable degradation rates matching the tissue formation to achieve the desired restoration. Currently, GTR membranes based on biodegradable polymers (mainly xenogenic collagen) are commercially available, nevertheless, those membranes present poor mechanical properties and high solubility in physiological conditions resulting in difficult clinical manipulation and early rupture at the tissue defect site during GTR treatment [3]. Another important challenge in GTR procedures are the infections generated by bacterial colonization at the membrane [4]. Post-operative infections and early membrane rupture are currently considered the major reasons for GTR failure in clinical applications [5,6].

Composite membranes fabricated by electrospinning can combine the properties of their different components and the intrinsic morphology of electrospun materials to result in biological, chemical and physical favorable features for tissue engineering. The electrospinning technique uses electrostatic forces to produce polymeric-based fibrillar membranes with interconnected porosity and fibers diameters ranging from tens of nanometers to few micrometers [7], mimicking the morphology of the extracellular matrix (ECM) and enhancing the viability, adhesion and proliferation of mammalian cells [7,8].

Polycaprolactone (PCL) is a synthetic semi-crystalline polymer approved by the US Food and Drug Administration (FDA) [9]. It has excellent biocompatibility and mechanical stability; however, its hydrophobic nature and lacking of biologically active functional groups limits its ability to promote cell adhesion, proliferation and migration [10]. On the other hand, gelatin (Gel) is a natural polymer derived from the partial hydrolysis of collagen, which is the main component of ECM, including periodontal connective tissue ECM [11,12]. It displays a good biological response since it has some of the functional groups present in collagen but produces lower immunogenicity and antigenicity than collagen [13–15]. Nonetheless, Gel dissolution and fast biodegradation in physiological conditions make it mechanically unstable and restrict its use in GTR membranes [10,16,17]. Blends of PCL and Gel can combine the intrinsic properties of both polymers resulting in materials with biologically favorable properties, specially blends with 30 w% Gel concentrations or higher [15,18,19], and modulated biodegradation rates, overcoming the respective disadvantages of PCL and Gel themselves [14,18–21].

GTR membranes with local antibacterial properties are expected to reduce the risk of infections allowing a bacteria-free environment for appropriate tissue regeneration [16]. Several polymeric membranes that can deliver antibiotics at the defect site have been investigated as an alternative to avoid infections during GTR procedures [22–24]. However, the use of antibiotics could increase the risk of developing antibiotics-resistant bacteria which is considered an important global problem [25]. Recently, the use of antibacterial nanoparticles (NPs) represents a promising strategy to face the increasing emergence of antibiotic-resistant bacteria [26]. Particularly, zinc oxide nanoparticles (ZnO-NPs) are "generally recognized as safe" by the FDA (21CFR182.8991) and have demonstrated antibacterial activity against a wide variety of bacteria,

including antibiotics-resistant strains [26–30]. By using the electrospinning technique, NPs can be embedded into polymeric matrices, controlling the undesirable burst release of NPs into the organism and taking advantage of the inherent high surface-area-to-volume-ratio of electrospun fibrillar membranes to maintain a high surface exposure of the NPs and consequently a high antibacterial activity [31]. A study conducted by E. A. Münchow et al. reported the antibacterial efficacy of PCL-Gel polymeric electrospun membranes loaded with ZnO-NPs against two oral bacteria; their results showed a clear inhibition of bacterial growth using ZnO-NPs concentrations of 5, 15 and 30 w% (relative to the total polymer weight) and a relatively good biocompatibility using human dental pulp stem cells [32]. However, despite NPs with antibacterial properties are promising therapeutic agents, there are still concerns by the possible long-term side effects generated by an excessive release of NPs into human tissues [33]. To address this, we fabricated electrospun composite fibers of PCL and Gel loaded with ZnO-NPs (PCL-G-Zn membranes) in low concentrations (1, 3 and 6 w%) using acetic acid as a green the sole common-solvent and aiming to develop biocompatible, biodegradable and mechanically stable membranes with local antibacterial properties and lower NPs concentrations. Degradation, water wettability, mechanical properties and thermal properties of PCL-G-Zn membranes were studied in terms of their micromorphology, atomic structure and elemental chemical composition. The ability of the PCL-G-Zn membranes for inhibiting planktonic bacterial growth and bacterial biofilm formation against *Staphylococcus aureus* (*S. aureus*) was studied. The ability of the membranes to sustain periodontal cells viability was evaluated exposing human osteoblasts (hFOB) and gingival fibroblast (hGF-1) to the membranes lixiviates.

2. Materials and Methods

2.1. Materials.

Polycaprolactone (PCL; Mn = 80,000 Da), Zinc oxide nanoparticles (ZnO-NPs), MTT ([3-(4,5-dimethylthiazol-2-yl)-2,5-diphenyltetrazolium bromide]) (MTT), 2-propanol 99% (ISO), dimethyl sulfoxide (DMSO), menadione and hemin were purchased from Sigma-Aldrich. Glacial acetic acid (AcAc; 99.5%) and Gelatin Type B derived from porcine skin (Gel) were purchased from J.T Baker. Dulbecco's Modified Eagle's Medium F12 (DMEM), Fetal Bovine Serum (FBS), penicillin/streptomycin 0.25%, trypsin–EDTA 0.25% and Phosphate Buffered Saline (PBS; pH = 7.4) were acquired from Gibco, and Trypticase Soy Broth (TSB) was purchased from BD Bioxon. *Staphylococcus aureus* (*S. aureus*; 25923™), human osteoblasts (hFOB; CRL-11372™), gingival fibroblasts (hGF-1; CRL-2014™), and geneticin were obtained from ATCC®

2.2. Fabrication of membranes.

Blend solutions of PCL and Gel were prepared by dissolving PCL (19% w/v) into AcAc and incorporating the appropriate amount of Gel to produce two PCL-Gel solutions with final PCL:Gel weight ratio of 70:30 or 55:45. Separately, adequate amounts of ZnO-NPs were weighed (1, 3 and 6 w%; relative to PCL content) and dispersed individually into PCL-Gel solutions to produce eight different PCL-Gel-ZnO solutions, that is, PCL:Gel (70:30) solutions with 0, 1, 3 and 6 wt% of ZnO-NPs, and PCL:Gel (55:45) solutions with 0, 1, 3 and 6 wt.% of ZnO-NPs. A solution of only PCL in AcAc (19% w/v) was also prepared. All solutions were stirred at 300 rpm for 48 h at room temperature (RT). For electrospinning, the PCL-Gel and PCL-Gel-ZnO solutions were independently pumped at 1 mL/h, with a needle-to-collector distance of 14 cm and using a

voltage of 14 kV. The PCL solution was pumped at the same solution feed rate but increasing the needle-to-collector distance and the voltage to 15 cm and 15 kV, respectively. Electrospinning was carried out using a horizontal equipment assembled in our laboratory where electrospun fibers (membranes) were collected on a static aluminum plate. After electrospinning, membranes were removed from the collector, double washed with EtOH (70%) and double distilled water (dd H_2O), dried at RT and sterilized under ultraviolet light (UV). Electrospun membranes were named accordingly to their composition as described in Table 1.

Table 1. Chemical composition of electrospun membranes.

Electrospun membrane	Chemical composition		
	PCL (wt.%)[a]	G (wt.%)[a]	ZnO NPs (wt.%)[b]
PCL	100	0	0
PCL-G30	70	30	0
PCL-G30-1Zn	70	30	1
PCL-G30-3Zn	70	30	3
PCL-G30-6Zn	70	30	6
PCL-G45	55	45	0
PCL-G45-1Zn	55	45	1
PCL-G45-3Zn	55	45	3
PCL-G45-6Zn	55	45	6

[a]wt.% according to total polymer content (PCL + Gel) in electrospinning solution. [b] wt.% according to total PCL content in electrospinning solution.

2.3. Physico-chemical and mechanical characterization of membranes.

The micromorphology of the membranes was characterized by Scanning Electron Microscope (SEM; JEOL-7600); fiber diameter distribution and surface pore size were estimated from SEM micrographs of carbon-coated membrane samples. Elemental chemical composition

was determined by Energy Dispersive X-Ray Spectrometry (EDS; Oxford X-Max 150) during SEM micrographs acquisition. Incorporation of ZnO-NPs into the PCL-G membranes was corroborated by bright field Transmission Electron Microscopy (TEM, PHILIPS CM 100).

Water wettability of the membranes was determined by measuring their water contact angles (WCA) via the static sessile drop method using a Ramé–Hart goniometer; WCA were measured at 1, 3, and 5 s after deposition of a 4 μL dd H_2O drop on the membranes surface.

Functional groups in the membranes were identified by Infrared Spectroscopy (FTIR) using an infrared spectrometer (Nicolet 880 FTIR) with Attenuated Total Reflection (ATR).

Mechanical properties of the membranes were determined through mechanical stress-strain tests (tension, 2 mm/min) using a universal test machine (INSTRON 4465); the elastic modulus (E), elongation at break (ϵ) and maximum tensile strength (σ_{max}) were determined.

The atomic structure of the membranes was determined by acquiring X-Ray diffraction (XRD) patterns using a PANalytical X'Celerator diffractometer with CuKα radiation in a 2θ configuration. Degree of crystallinity of the membranes ($\chi_{C\text{-}XRD}$) was calculated from XRD patterns according to [(Area of crystalline peaks $_{(110)\ and\ (200)}$)/(Area of crystalline peaks $_{(110)\ and\ (200)}$ + Area of amorphous peak)]x100; [34,35].

Thermal properties of the membranes were studied by Thermogravimetry (TGA) and Differential Scanning Calorimetric (DSC) analysis under nitrogen atmosphere. TGA measurements were performed using a thermogravimetric analyzer (TGA2950; TA Instruments) by heating the sample from RT to 700 °C at a heating rate of 10 °C/min. DSC measurements were acquired using a DSC equipment (Q2000; TA Instruments) from -90 to 150 °C at a heating rate of 10 °C/min. Quench cooling was applied after first heating scan and immediately a second heating scan was

completed. Degree of crystallinity of the membranes ($\chi_{C\text{-}DSC}$) was calculated from DSC thermograms according to [36] ($\Delta Hm / \Delta H^0_m$)x100, where, ΔH_m was the sample melting enthalpy and ΔH^0_m was the melting enthalpy of 100% crystalline PCL ($\Delta H^0_{m(PCL)}$) = 142.0 J/g [37,38]).

To evaluate the degradation of the membranes, dry samples (1 cm in diameter) were weighed (W_0), immersed in PBS and incubated at 37 °C and 120 rpm. After 1, 2, 3, 4, 9, 17, 24 and 31 days, samples were washed with dd H_2O, dried and weighed (W_1). Weight loss (W_{loss}) percentage was estimated as [(W_0-W_1)/W_0]X100.

To estimate the cumulative Zn released from the PCL-G-Zn membranes, individual samples (1 cm in diameter) were immersed in 1 mL of MilliQ-H_2O and incubated at 37°C and 120 rpm. After 1, 3 and 7 days of incubation, the samples were taken out from the water and immersed again in 1 mL of fresh MilliQ-H_2O, the Zn concentration in collected supernatants at 1, 3 and 7 days was measured by Inductively Coupled Plasma Mass Spectrometry (ICP-MS; iCAP Q, Thermo Scientific).

2.4. In vitro antibacterial activity of composite membranes.

The antibacterial activity of the membranes was determined by evaluating the planktonic and biofilm growth inhibition of *S. aureus*. Pure cultures of *S. aureus* were collected from agar plates and resuspended in TSB supplemented with menadione 1% v/v and hemin 1% v/v. Bacterial solution was adjusted to optical density (O.D.) of 1 at $\lambda = 600$ nm (BioPhotometer D30). Circular sterilized samples (8 mm in diameter) of the membranes were placed in 48-culture well plates by triplicate, individually inoculated with 1 x10^5 cells/mL and incubated at 37 °C in an orbital shaker incubator (Cleaver Scientific Ltd) at 120 rpm. After 1, 3 and 7 days of incubation, the capability of the membranes to inhibit planktonic bacterial growth was estimated by

measuring the turbidity of the inoculated culture media at λ = 595 nm in a FilterMaxF5 multi-mode microplate reader (Molecular Devices, USA). Turbidity (%) was calculated according to $[(O.D_{A1}-O.D_{A2})/(O.D_{B1}-O.D_{B2})] \times 100$, where, $O.D._{A1}$ = absorbance of supernatants from bacteria incubation with the membranes, $O.D._{B1}$ = absorbance of supernatants from bacteria incubation with no membranes (negative control), $O.D._{A2}$ = absorbance of supernatants from membranes incubation with no bacteria, and $O.D._{B2}$ = absorbance of culture media only.

The capacity of the membranes to prevent biofilm growth was evaluated by MTT assay. Bacteria-incubated membranes were rinsed once with fresh supplemented TSB to detach loosely attached bacteria. Then, membranes were transferred to a new culture well plate and incubated with a 1:10 solution of MTT:culture-media for 3 h at 37 °C and 120 rpm to asses viability of bacteria cells adhered on the membranes. After MTT incubation, bacteria-metabolized formazan crystals were solubilized in a ISO:DMSO solution (1:1) and absorbance at λ = 570 nm was read using the FilterMax F5. Bacteria viability (%) was estimated according to $[(O.D_{A1}-O.D_{A2})/(O.D_{B1}-O.D_{B2})] \times 100$, where $O.D._{A1}$ = absorbance of solubilized-formazan from bacteria adhered on PCL-G or PCL-G-Zn membranes, $O.D._{B1}$ = absorbance of solubilized formazan from bacteria adhered on PCL membranes (as negative control since they are not expected to prevent bacterial adhesion), $O.D._{A2}$ = absorbance reads from MTT-incubated corresponding PCL-G or PCL-G-Zn membranes with no bacteria, and $O.D._{B2}$ = absorbance reads from PCL membranes with no bacteria.

Selected PCL, PCL-G30, PCL-G45, PCL-G30-1Zn and PCL-G45-1Zn membranes used for antibacterial testing were fixed (2% glutaraldehyde at 4 °C), washed with PBS, dehydrated

through a series of graded ethanol solutions and observed by SEM (JSM 7600F, JEOL) to qualitatively assess the membranes stability and the bacterial adhesion on their surface.

2.5. In vitro biocompatibility of composite membranes.

The toxicity of lixiviate products from the membranes was tested using hFOB and hGF-1. Confluent cell cultures were treated with 0.05% trypsin-EDTA, collected by centrifugation, and seeded at a density of 1 x10^4 cells/well on 24-well culture plates with DMEM supplemented with 10% v/v FBS and 1% v/v penicillin/streptomycin (0.25%) or 3% geneticin for hGF-1 or hFOB, respectively. After 1 day of incubation at 37 °C and 5% CO_2, sterilized membrane samples (diameter = 6 mm) were individually placed in hanging cell culture inserts (Millicell®) and placed on the culture 24-wells plates where cells were seeded 24 h before; culture plates were put back in the incubator. After 1 day of culture, hanging inserts were removed and cell viability was assessed by MTT assay using the same protocol described above. Percentage of cell viability was estimated according to $[(O.D_{A1}-O.D_{A2})/(O.D_{B1}-O.D_{B2})]\times100$, where, *$O.D._{A1}$* = absorbance of solubilized formazan from cells cultured in the presence of membranes lixiviates, *$O.D._{B1}$* = absorbance of solubilized formazan from cells cultured in the presence of no membranes (positive control), and *$O.D._{A2}$* = *$O.D._{B2}$* = absorbance of ISO:DMSO solution.

*2.6. Statistical analysis*

The biological experiments were conducted twice using three samples of each group. Results are expressed as mean values ± standard deviation. Results were plotted using Origin 9.0 Software. The statistical significance was determined by one-way analysis of variance (ANOVA), followed by a Tukey's multiple comparison test; considering $p < 0.05$ as statistically significant.

3. Results

3.1. Physico-chemical and mechanical properties of membranes.

Macroscopically, the membranes were white in color, flexible, soft to the touch and ≈ 0.4 mm in thickness. (Supplementary Figure S1). Microscopically, the membranes showed a randomly oriented fibrillar structure with rough surface fibers of average diameters (d) ranging from 1.38 to 0.41 μm (Figure 1), and interconnected porosity with pore size ranging from 138.7 to 4.5 μm^2 (Table 2). Addition of Gel to the membranes, PCL-G, narrowed the average fiber diameter and presented a more homogeneous, in fibers diameter, morphology in comparison to PCL membranes (i.e. the fiber diameters distribution was lower dispersed; Supplementary Figure S2). In the same fashion, the addition of ZnO-NPs to the membranes, decreased the average fiber diameter in comparison to their corresponding PCL-G membranes. The average pore size of the PCL-G membranes was larger than that of the PCL membranes. In contrast, addition of ZnO-NPs to the membranes, significantly decreased the pore size, in comparison to PCL-G or PCL membranes (Table 2).
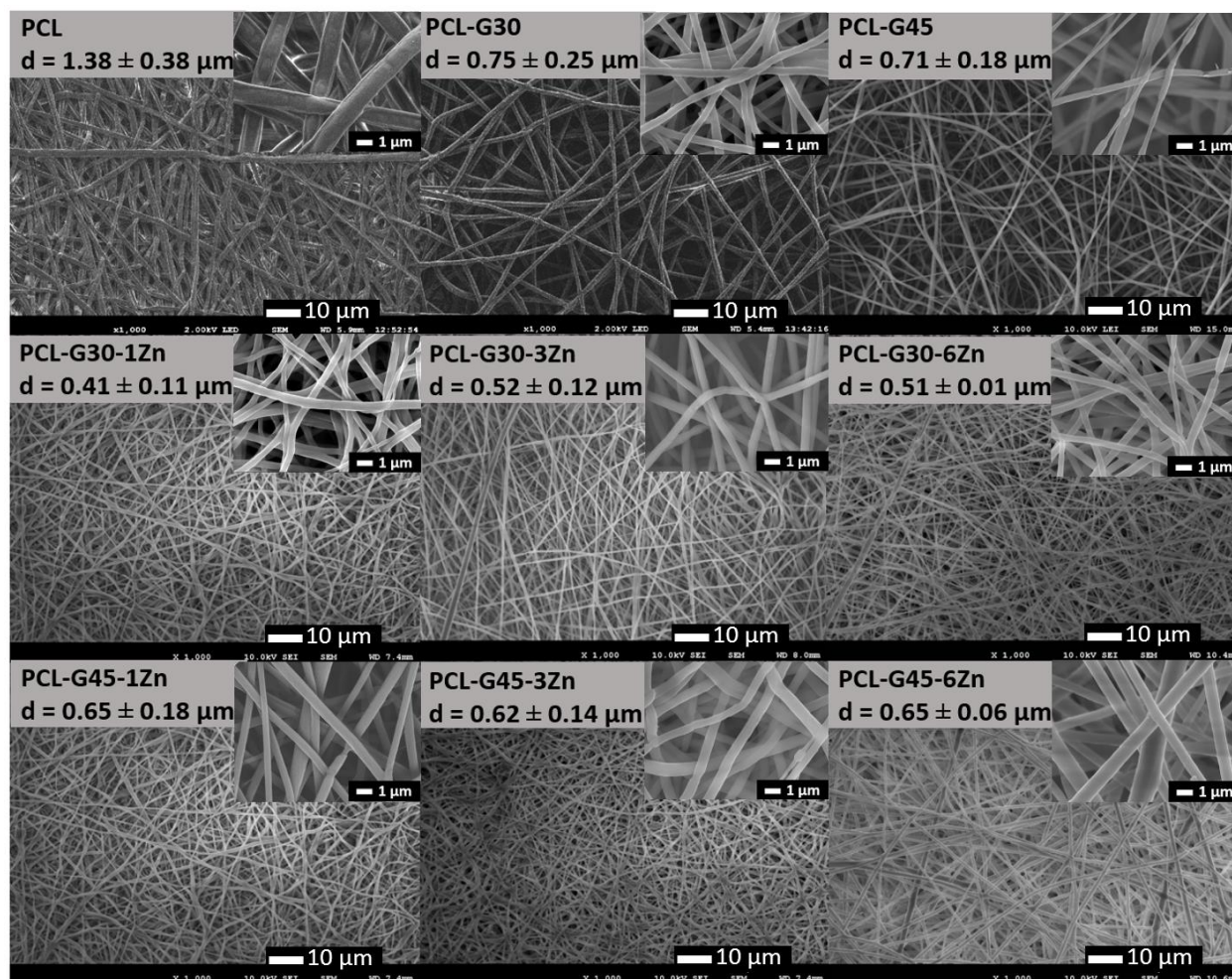
Figure 1. Representative SEM micrographs and fiber average diameters of PCL, PCL-G and PCL-G-Zn membranes.

Table 2 also presents the EDS and WCA measurements. The EDS analysis showed high concentrations of C and O in the PCL and PCL-G membranes and confirmed the corresponding Zn w% concentration in the PCL-G-Zn membranes. Regarding WCA, the PCL membranes showed hydrophobic character (WCA ≈ 130°) while the PCL-G membranes showed hydrophilic character, WCA ≈ 60°. WCA angles PCL-G membranes increased slightly with the incorporation of ZnO-NPs, but remained hydrophilic (WCA < 90).

Table 2. Average pore size of the membranes estimated from SEM micrographs, elemental composition as obtained from Electron Dispersive Spectroscopy, average water contact angle measured at 1 s, 3 s and 5 s after droplet deposition on the membranes.

Electrospun membrane	Pore size (μm²)	Elemental composition as determined from EDS (wt.%)			Water contact angle (°)		
		C	O	Zn	1s	3s	5s
PCL	71.8 ± 37.4	71.69	28.31	-	132.8 ± 2.4	130.9 ± 2.5	130.5 ± 2.6
PCL-G30	138.7 ± 74.2	67.45	32.55	-	66.5 ± 1.7	41.0 ± 0.8	31.8 ± 0.1
PCL-G30-1Zn	24.3 ± 16.7	63.37	35.61	1.02	73.5 ± 3.1	57.5 ± 0.7	41.6 ± 0.0
PCL-G30-3Zn	36.6 ± 19.9	68.26	28.53	3.21	77.0 ± 1.4	74.4 ± 2.5	65.0 ± 0.7
PCL-G30-6Zn	21.7 ± 7.7	68.74	25.88	5.39	89.3 ± 1.1	82.1 ± 0.8	77.2 ± 0.5
PCL-G45	115.6 ± 63.5	68.12	31.88	-	56.9 ± 7.3	19.4 ± 1.9	14.8 ± 0.2
PCL-G45-1Zn	12.4 ± 10.3	67.30	32.01	0.70	70.6 ± 0.4	49.2 ± 6.7	46.7 ± 4.7
PCL-G45-3Zn	4.5 ± 2.7	66.83	29.90	3.27	79.2 ± 0.5	64.5 ± 2.7	62.4 ± 3.6
PCL-G45-6Zn	5.2 ± 3.3	64.80	28.55	6.65	79.4 ± 0.6	66.1 ± 3.6	65.2 ± 0.3

Bright field TEM micrographs (Figure 2) showed dark nanostructures embedded in the PCL-G-Zn fibers, suggesting (according to EDS results showing the elemental composition of the membranes as C, O and Zn) the successful incorporation of the ZnO-NPs in the membranes.
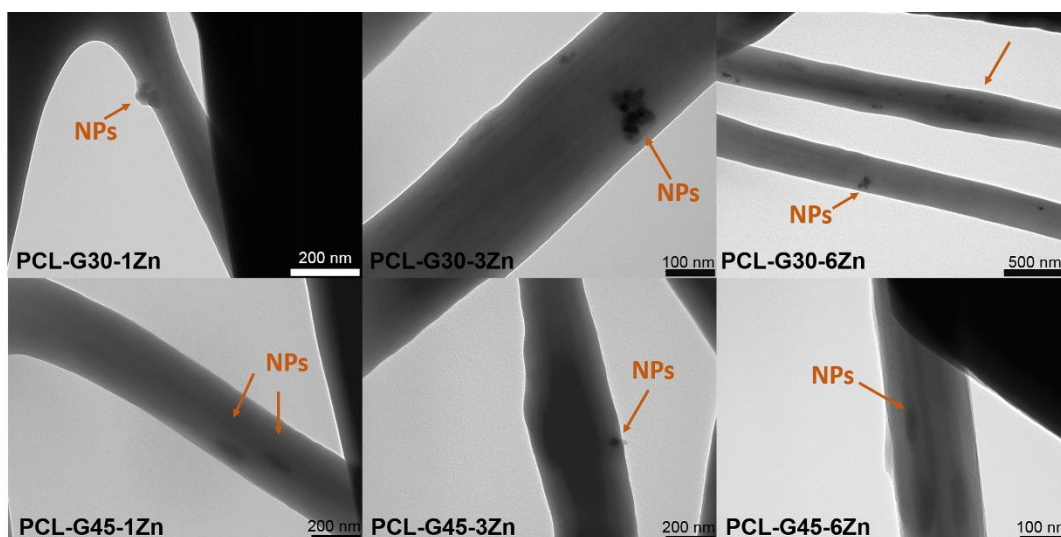
Figure 2. Representative TEM micrographs of PCL-G-Zn membranes.

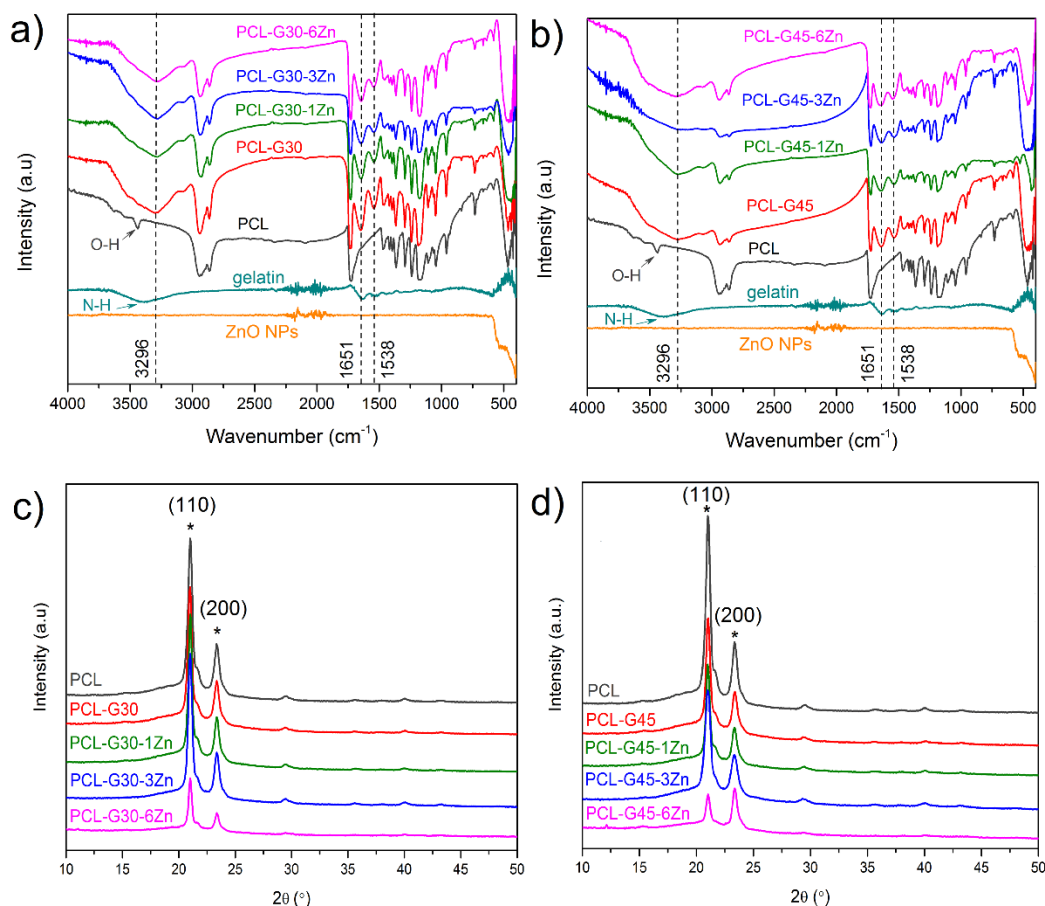FTIR spectra of the PCL-G and PCL-G-Zn membranes (Figures 3a and 3b) showed the characteristic bands of PCL at 2945 cm^{-1} ($v_{as}CH_2$), 2859 cm^{-1} (v_sCH_2), 1731 cm^{-1} ($vC=O$), 1294 cm^{-1} ($vC-C$), 1240 cm^{-1} ($v_{as}C-O-C$), 1175 cm^{-1} (v_sC-O-C) and 1045 cm^{-1} ($vC-O$), and the characteristic bands of Gel at 1651 cm^{-1} ($vC=O$, amide I) and 1538 cm^{-1} ($\delta N-H$, amide II) [39]. FTIR spectra of the PCL membranes showed a band at $\approx$ 3420 corresponding to O-H groups, posibly indicating a slight degradation of the PCL molecules possibly induced by the acidity of the AcAc (pH $\approx$ 2.4) during the electrospinning solution [40]. O-H groups in the PCL are expected to increase its predisposition to form hydrogen bonds with the N-H groups of the Gel molecules, which can be confirmed by the FTIR broad band centered at 3296 cm^{-1} observed in the FTIR spectra of the PCL-G membranes that can be attributed to the overlapping of the O-H and N-H groups [41]. The FTIR spectra of the PCL-G-Zn membranes did not show any clear band corresponding to Zn-O, mainly because those bands are expected to appear at wavenumbers below 550 cm^{-1} and thus, they could easily be overlapped by the stronger bands of PCL at similar wavenumbers.

XRD patterns of all membranes (Figures 3c and 3d) showed the characteristic two diffraction peaks of the semi-crystalline PCL structure at 2Θ = 21.11° and 23.99° corresponding to the (110) and (200) planes [42]. A decrease in χ_{C-XRD} was observed as the Gel content increased in PCL-G membranes and with the increasing ZnO-NPs concentration in PCL-G-Zn membranes (Table 4). The peaks deconvolution of the XRD patterns for the χ_{C-XRD} estimations of membranes is shown in the Supplementary Figure S3.

Figure 3. FTIR-spectra of (a) pristine Gel and PCL, PCL-G30 and PCL-G30-Zn membranes, and (b) pristine Gel and PCL, PCL-G45 and PCL-G45-Zn membranes. XRD patterns of (c) PCL, PCL-G30 and PCL-G30-Zn membranes, and (d) PCL-G45 and PCL-G45-Zn membranes.

The mechanical parameters of the membranes calculated from the obtained stress-strain curves (Supplementary Figure S4) are reported in Table 3. Gel and ZnO-NPs addition to the membranes increased their elastic modulus in a concentration-dependent manner in comparison to PCL membranes. The elongation at break, ε, of the membranes significantly decreased from 238.25% to 1.53% as Gel concentration increased. Only for the PCL-30G membranes, the concentration of ZnO-NPs played an important role leading to a maximum ε for the 1 w%; PCL-30G-1Zn sample. On the other hand, the maximum tensile strength, σ_{max}, decreased with the Gel

17

concentration, PCL > PCL-30G > PCL45G, and the addition of ZnO-NPs did not significantly modify the σ_{max} for neither PCL-G30-Zn nor PCL-G45-Zn membranes.

Table 3. Mechanical parameters calculated from the strain-stress curves of the membranes: elastic modulus, E; elongation at break, ε; maximum tensile strength, σ_{max}.

Electrospun membrane	E (MPa)	ε at break (%)	σ_{max} (MPa)
PCL	6.09 ± 3.10	238.25 ± 59.12	2.27 ± 0.94
PCL-G30	12.66 ± 2.63	62.67 ± 22.03	1.46 ± 0.18
PCL-G30-1Zn	12.74 ± 3.05	117.78 ± 22.60	1.67 ± 0.28
PCL-G30-3Zn	24.78 ± 7.34	70.33 ± 28.50	1.63 ± 0.19
PCL-G30-6Zn	26.94 ± 7.36	14.52 ± 3.56	1.43 ± 0.09
PCL-G45	49.56 ± 20.72	1.53 ± 0.15	0.65 ± 0.29
PCL-G45-1Zn	41.91 ± 23.65	1.23 ± 0.25	0.43 ± 0.27
PCL-G45-3Zn	41.91 ± 23.64	1.34 ± 0.21	0.58 ± 0.29
PCL-G45-6Zn	65.38 ± 17.42	1.23 ± 0.32	0.75 ± 0.40

Thermal parameters of the membranes and of pristine Gel from TGA curves (Supplementary Figure S5) are summarized in Table 4. PCL showed a single weight loss step at a temperature of maximum weight loss rate (T_{max}) of 394 °C. Pristine Gel showed a first weight loss step at T_{max} of 67 °C followed by a broad degradation step, where two weight loss peaks were identified at T_{max} of 288 °C and 317 °C. PCL-G and PCL-G-Zn membranes exhibited an initial weight loss at $T_{max} \approx$ 35–32 °C, followed by two weight loss peaks at $T_{max} \approx$ 389–379 °C and at $T_{max} \approx$ 325–316 °C. PCL-G30-6Zn and PCL-G45-6Zn membranes exhibited additional weight loss peaks at T_{max} = 227 °C and 213 °C, respectively.

Table 4. Thermogravimetric characterization and calorimetric properties of pristine Gel and PCL-G and PCL-G-Zn nanocomposite membranes.

Material	Temperature of maximum weight loss rate for each degradation step — T_{max} (°C)				T_m[a] (°C)	ΔH_m[b] (J/g)	$\chi_{C\text{-}DSC}$[d] (%)	$\chi_{C\text{-}XRD}$[e] (%)
Pristine gelatin	67	288	317	-	-	-	-	-
PCL	-	-	-	394	54	70	49	46
PCL-G30	35	-	324	389	56	50	35	40
PCL-G30-1Zn	35	-	324	389	56	45	33	39
PCL-G30-3Zn	35	-	324	389	56	44	31	39
PCL-G30-6Zn	33	227	317	376	56	38	28	37
PCL-G45	32	-	318	387	56	41	29	35
PCL-G45-1Zn	32	-	318	387	56	41	29	34
PCL-G45-3Zn	32	-	318	387	56	40	29	36
PCL-G45-6Zn	35	213	316	381	56	36	24	30

[a]melting temperature; [b]melting enthalpy; [c]melting enthalpy per gram of PCL, [d]degree of crystallinity from melting enthalpy and [e]degree of crystallinity from XRD patterns.

Calorimetric properties of the membranes from heating DSC scans (Supplementary Figure S6) are summarized in Table 4. A unique endothermal peak corresponding to the melting temperature (Tm) of the PCL component was detected at 55 °C for all membranes. The endothermic melting enthalpy (ΔHm) of the PCL-G membranes decreased as the Gel concentration increased and with the presence of 6 w% ZnO-NPs. The presence of 1 and 3 w% of ZnO-NPs in the membranes did not alter the ΔHm values, indicating that $\chi_{C\text{-}DSC}$ only decreased with increasing Gel concentration and with the highest ZnO NPs concentration studied (PCL-30G-6Zn and PCL-45G-6Zn) in the membranes.

Figure 4 shows the weight loss of the membranes as a function of incubation time and the cumulative Zn released from the PCL-G-Zn membranes. In Figure 4a could be seen that the PCL membranes did not show significant degradation (W_{loss} < 8%) after 31 days of incubation, while the PCL-G and PCL-G-Zn membranes experienced a significantly larger degradation (W_{loss} ≈ 35 - 46%), which was faster during the first 3 days. The W_{loss} was slightly affected by the ZnO Nps concentration for the PCL-G30-Zn membranes, where W_{loss} slightly increased with the increment of ZnO content in the PCL-30G membranes. For the PCL-G45-Zn membranes no significant differences were observed in W_{loss} with the increasing content of ZnO-NPs (Figure 4b).

The release of Zn in water increased over time as ZnO-NPs concentration increased in the PCL-G membranes, independently of the Gel concentration (Figure 4c and 4d). However, the Zn amount released from all membranes gradually diminished with the incubation time. The release of Zn from PCL-G45 membranes with 3 and 6 w% of ZnO-NPs was significantly higher than that from their corresponding PCL-G30 membranes, while the Zn amount released from the PCL-G30 and PCL-G45 membranes with 1w% of ZnO-NPs was comparable.
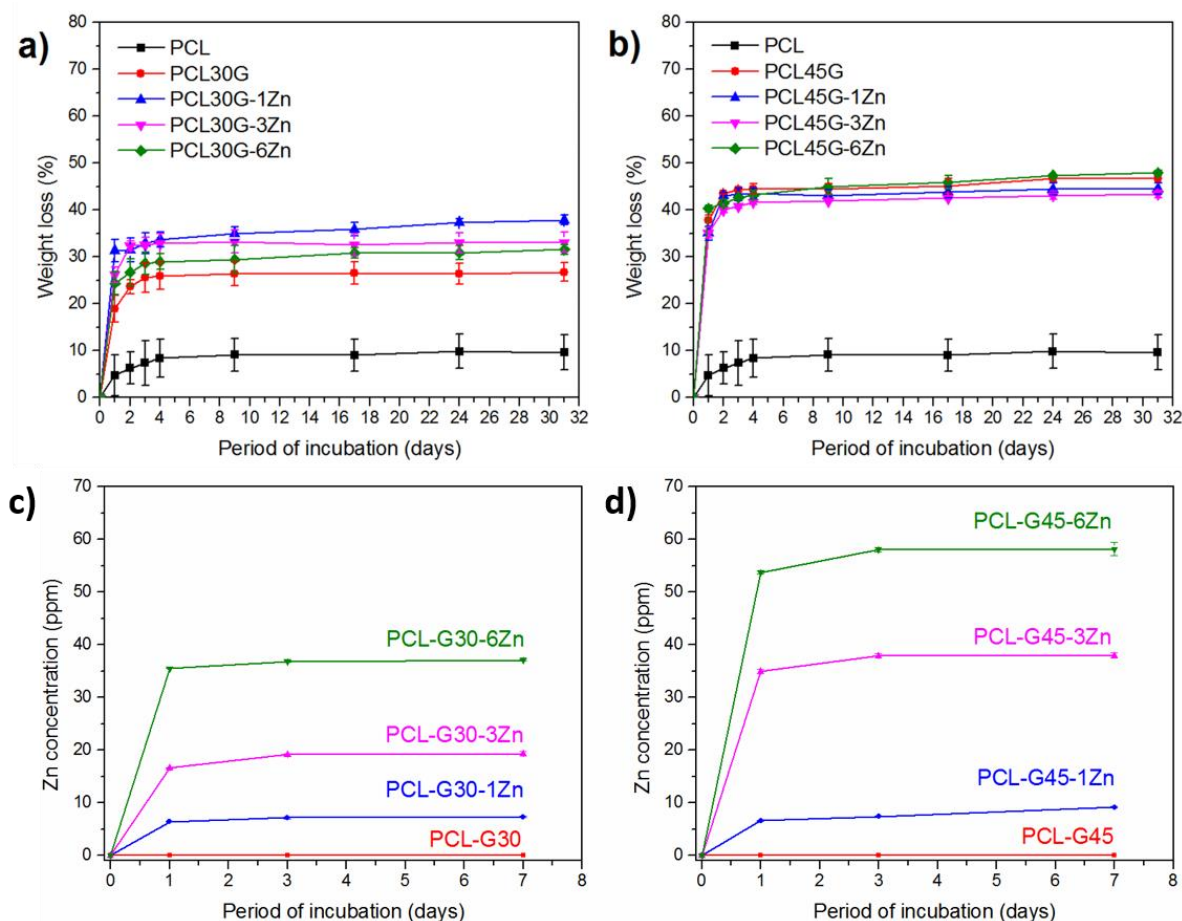
Figure 4. Weight loss percentage over time of (a) PCL, PCL-G30 and PCL-G30-Zn, and of (b) PCL, PCL-G45 and PCL-G45-Zn membranes incubated in PBS at 37 °C and 120 rpm. Concentration of cumulative Zn released from (c) PCL-G30-Zn membranes and (d) PCL-G45-Zn membranes after 1, 3 and 7 days of incubation in water at 37 °C and 120 rpm measured by ICP-MS.

The inhibition of planktonic bacterial growth measured by the turbidity assay at 1, 3 and 7 days of incubation (Figure 5a), showed that the PCL-G membranes (PCL-G30 and PCL-G45) slightly reduced turbidity over time compared to the PCL membrane. Even more, the addition of ZnO-NPs to the PCL-G membranes significantly reduced planktonic growth at the three incubation times; moreover, the bacterial growth inhibition was effective independently of the ZnO-NPs concentration. On the other hand, a significantly decrease in the viability of the attached

bacteria on the membranes (Figure 5b) was observed with the addition of ZnO-NPs to PCL-G membranes. Although no clear trend could be inferred regarding the NPs concentration at the different incubation times, significant reduced levels of viable bacteria were detected on the membranes loaded with ZnO-NPs at 7 days of incubation.
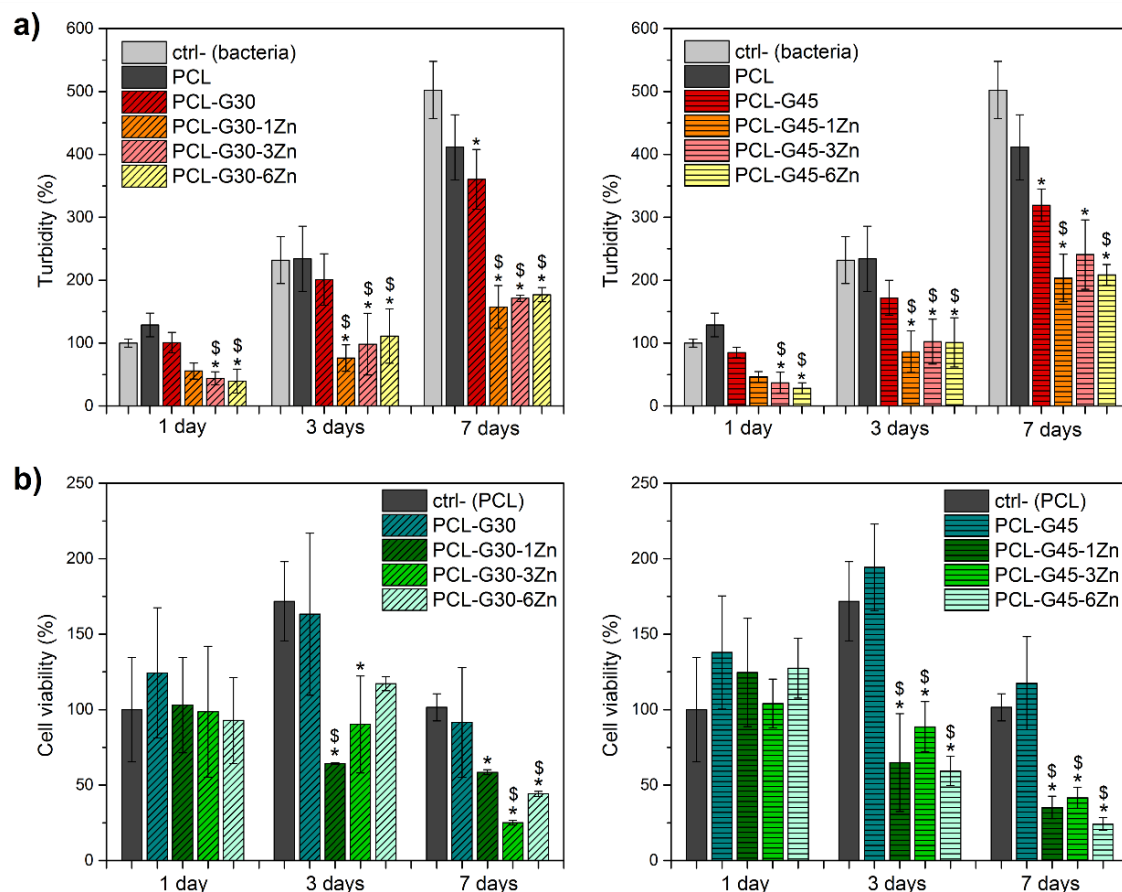
Figure 5. (a) Bacterial growth on the broth medium in the presence of the PCL, PCL-G or PCL-G-Zn membranes measured by the turbidity assay (Turbidity percentage) and (b) Cell viability of the adhered bacteria on the PCL, PCL-G and PCL-G-Zn membranes measured by the MTT assay, after 1, 3 and 7 days of incubation. *****, p < 0.05 for ctrl- (bacteria in presence of no membrane) *vs.* all membranes and **$**, p < 0.05 for PCL-30G or PCL-45G membranes *vs.* their corresponding membrane loaded with 1, 3 or 6 wt.% Zn NPs. All statistical comparisons were performed using the same incubation time.

Representative SEM micrographs of the PCL, PCL-G and PCL-G-1Zn membranes at 7 days of bacterial incubation are shown in Figure 6. PCL-G-Zn with only 1 w% of ZnO-NPs presented an important reduction of the adhered bacteria in comparison to membranes with no ZnO NPs added. Moreover, the SEM micrographs showed that the fibrillar structure of the membranes was preserved after the 7 days in culture with bacteria.
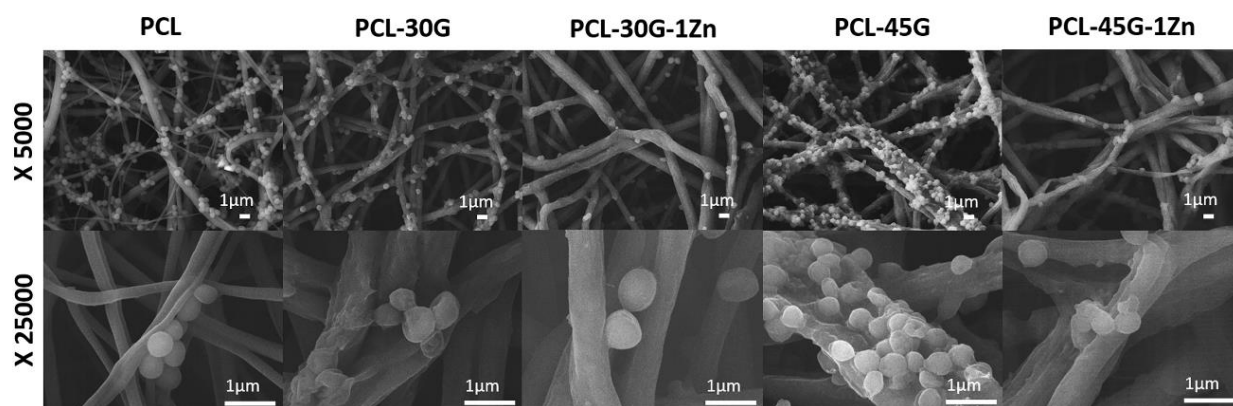
Figure 6. Representative SEM micrographs of PCL, PCL-G30, PCL-30G-1Zn, PCL-G45, and PCL-G45-1Zn membranes after 7 days of bacterial inoculation.

3.3. In vitro biocompatibility of membranes.

The viability (as determined by the MTT assays) of hFOB and hGF-1 exposed to the membranes lixiviates is shown in Figure 7. In general, both cell types did not show significant differences in the percentage of cell viability (CV%) when exposed to the release products of the PCL and PCL-G membranes in comparison to the positive control, but the presence of ZnO-NPs in the membranes decreased the CV% in a Zn concentration depended manner. However, both cell types exhibited more than 85% of CV% after 24 h of culture in the presence of PCL-30G-1Zn or PCL-45G-1Zn membranes lixiviates. It is interesting to notice that hFOB were less sensitive to the

ZnO-NPs, since only hFOB cells exposed to the PCL-45G-6Zn membranes lixiviates presented less than the 50% of cell viability in comparison to the positive control. On the contrary, hGF-1 cells showed a significantly decrease in the CV% when exposed to PCL-G membranes with 3 and 6 w% of ZnO-NPs, in comparison to the positive control.
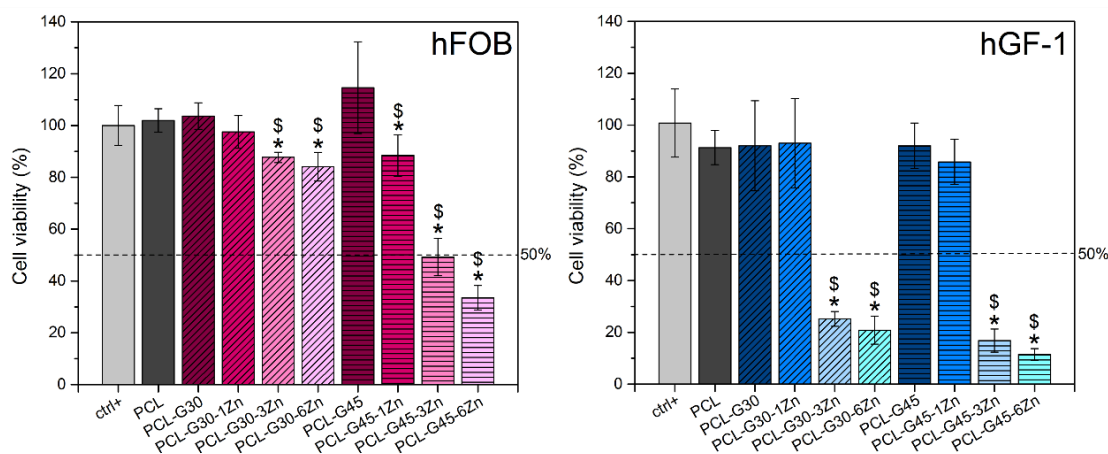
Figure 7. Viability of human osteoblasts (hFOB) and human gingival fibroblasts (hGF-1) exposed to the PCL, PCL-G blended or PCL-G-Zn membranes lixiviates, estimated by MTT assay after 1 day of incubation. *****, $p < 0.05$ vs. ctrl+; and **$**, $p < 0.05$ vs. PCL-30G or PCL-45G membranes without NPs.

4. Discussion

Phase-separation of PCL and Gel mixtures, due to their dissimilar physical-chemical properties, negatively affects their electrospinning process generating poorly blended inhomogeneous membranes. In the current study, fibrillar membranes of PCL and Gel loaded with different amounts of ZnO-NPs were fabricated by the electrospinning technique using AcAc. Worth mentioning that AcAc is considered a "green" solvent, since it is less toxic than other solvents, such as hexafluoro-2-propanol (HFP) or trifluoroethanol (TFE), frequently used for miscible Gel-PCL electrospinning solutions [32,43]. As a consequence of the synthesis conditions, hydrogen bonds between PCL and Gel were exhibited by the FTIR, this hydrogen bonding influenced the

24

structural and mechanical properties of the membranes. The decrement of the average fiber

diameter of the PCL-G membranes was Gel concentration-dependent and it might be attributed

to the increment of charge density of the PCL-Gel electrospinning solutions in comparison to the

PCL-only solution [44]. The amino groups in the amphoteric Gel molecules can be easily

protonated at pH below their isoelectric point (pH ≈ 2.4 for AcAc) increasing the charge density

and conductivity of the electrospinning solution, effect not expected for the PCL solution since it

is a non-ionic molecule [45]. During the electrospinning process, the increased charge density

and conductivity in the jet, causes the jet to elongate by electrical forces producing narrower

fibers [46]. A similar reductive effect in the average fiber diameter of PCL-G membranes was

observed when the ZnO-NPs were added. The incorporation Zn-based NPs in the PCL-G-Zn

membranes was confirmed by TEM and EDS, hence, it can be assumed that ZnO-NPs were

successfully embedded in the PCL-G membranes. It is important to mention that in a previous

work developing PCL/ZnO-NPs membranes, we observed the formation of zinc acetate after a

partial reaction of the ZnO-NPs and AcAc in electrospinning solutions [47]; however, in the

present work there was no evidence of a similar reaction, may be due to the smaller ZnO-NPs

concentrations (preventing the observation of really small Zn acetate FTIR bands or XRD peaks)

or a particular effect of the Gel in the present membranes. The addition of ZnO-NPs in the

electrospinning solutions can increase the number of ions, increasing the charge density of the

PCL-G-Zn solutions compared to PCL-G solutions, resulting in even narrower fibers. The average

pore size of PCL-G membranes drastically decreased with the presence of ZnO-NPs, this

phenomenon can be attributed to the effect of reduced fiber diameter. Sanders et al.

theoretically demonstrated that smaller fiber diameters increase the number of fibers crossings

and decrease its distance, creating a smaller pore size [48]. Interestingly, the fiber diameter of the PCL-G membranes decreased with the presence of the Gel, but their average pore size was larger than that of the PCL membranes. The cause of this phenomenon is no clear; however, it was hypothesized that the dominant phenomenon that produced the pore size of PCL-G membranes was the charge-charge repulsion between fibers when they were deposited on the collector during the electrospinning process. As the charge density of the PCL-Gel electrospinning solutions increased in comparison to the PCL-only solution, the generated charge-charge electrostatic repulsion between the charged surface of the fibers also increased, facilitating their separation and increasing the pore-size of the PCL-G membranes in comparison to PCL membranes. The repulsion phenomenon did not considerably influence the expected relation between pore sized and fiber diameter of the PCL-G and PCL-G-Zn membranes, possibly because of the difference in the charge densities between the PCL-Gel and PCL-Gel-ZnO solutions.

The interconnected porosity is an essential factor when designing GTR membranes. In the current work, the intrinsic interconnectivity and average pore size of the PCL-G-Zn composite membranes (ranging from 4.5 to 36.6 μm^2) are expected to be large enough to permit the diffusion of physiological nutrients but small enough to act as cellular barrier [49].

Other relevant characteristic was the change from the hydrophobic to hydrophilic character for the PCL-G membranes in comparison to PCL membranes. Since the GTR membranes will be in direct contact with physiological fluids, hydrophilic surfaces are preferred to promote cell proliferation and to enhance tissue regeneration [50,51]. The addition of ZnO-NPs increased the WCA, but the hydrophilic character remained in all the PCL-G-Zn membranes. This could be explained by possible physical interactions (van der Waals forces) between the PCL or/and the

Gel molecules and the ZnO-NPs that could reduce the surface energy of the membranes and consequently their wettability [52]. Another possible explanation is the smaller pore size of PCL-G-Zn membranes compared with their corresponding PCL-G membranes, that might affect the easy distribution/absorption of water droplets on the membranes [53].

In terms of their thermal degradation properties, PCL-G and PCL-G-Zn membranes showed an initial small weight loss peak that can be attributed to the evaporation of absorbed water mostly from the highly hydrophilic Gel component. The second main weight loss peak corresponded to the rupture of PCL chains and depolymerization of PCL molecules [54]. The last weight loss peak can be ascribed to Gel molecules degradation due to protein chain breakage and peptide bonds rupture [55,56]. Therefore, thermal degradation of the membranes displayed the contribution of both polymeric components of the membranes, indicating a good blend composition. Interestingly, the PCL-G-Zn membranes with the highest ZnO-NPs content (PCL-30G-6Zn and PCl-45G-6Zn) showed an additional weight loss peak at lower temperatures, which might have been caused for an increase in the chain mobility due to a weak interaction between the polymer matrix and the ZnO-NPs [57,58]. All membranes exhibited a unique melting endothermic peak corresponding to the semi-crystalline PCL component. The ΔH_m of PCL-G membranes decreased as the Gel concentration increased, but the presence of 1 and 3 w% ZnO-NPs did not affect the ΔH_m values within the experimental error. Only the presence of 6 w% of ZnO-NPs decreased the ΔH_m value of the membranes, consequently, the crystallinity only decreased with increasing concentration of the amorphous component (Gel) and with the increment of ZnO-NPs concentration, this result was confirmed by XRD analysis. Diffraction peaks from ZnO-NPs were not observed in the XRD patterns of the PCL-G-Zn membranes, possibly

because NPs concentration is too small as compared to the overall polymeric weight of the membranes.

The PCL-G and PCL-G-Zn membranes developed in the present study exhibited appropriate mechanical stability. Compared with three commercial collagen membranes [59], the elastic modulus of the present membranes (E ≈ 6-65 MPa) was lower than the elastic modulus of the three reported commercial membranes (E ≈ 90-700 MPa), reflecting higher flexibility. Accordingly, the elongation at break of PCL-30G-Zn composite membranes (ε ≈ 14 - 117 %) was higher than that of reported commercial collagen membranes (ε ≈ 5.6 - 7.9 %). The higher plasticity of PCL-30G-Zn membranes could confer them better structural integrity during GTR treatment. Although the tensile strength of the PCL-G30-Zn membranes (σ_{max} = 1.43 - 1.67 MPa) was lower than that of commercially available collagen membranes (σ_{max} = 5.33 - 22.5 MPa), they met the mechanical requirements for their clinically use in GTR procedures as they are not subjected to high tensile strength when are immobilized at the defect site. Thus, the PCL-G30-Zn membranes developed in the present work have adequate mechanical properties to offer good clinical manipulation and excellent conformability to the defect site.

The degradation (weight loss) of the PCL-G membranes was significantly larger than that of the PCL membranes. Total weight loss after 3 days of incubation corresponded to 30% and 45% for PCL-30G- and PCL-45G-based membranes respectively, and it can be mainly attributed to the rapid Gel solubilization in aqueous media [60]. To confirm this, a Biuret assay was performed (Supplementary Figure S7), where it was confirmed that dissolution of ≈ 90-100% of Gel contained in the PCL-G membranes (30 w% and 45 w% of total mass for PCL-30G- and PCl-45G-based membranes, respectively) occurred during the first three days of incubation.

Furthermore, the higher wettability of PCL-G membranes compared with PCL membranes facilitated water surface interaction and consequently could also have increased hydrolytic degradation of PCL [54]. After day 3 of incubation, the membranes weight loss occurred at a lower rate and thus representing (up to day 31) enough membranes' integrity stability time to allow the bone cell repopulation needed for regeneration of the defect site during GTR procedures. Iglhaut et al. reported that bone cell migration reaches their peak after 7 days of surgery, with a mitotic activity decreased to nearly normal levels by the end of the third week [61]. The period in which GTR membranes must remain intact depends on the defect depth, the longest treatments in which the membranes are used are that of root coverage which would require membranes to remain mechanically stable from 6 to 24 months post-membrane implantation [12,62].

Bacterial colonization in the defect site and on the membranes are known to significantly compromise the outcome of GTR procedures. The antibacterial results demonstrated that present PCL-G-Zn membranes possessed antibacterial activity against *S. aureus*, a strain that has been found in the oral cavity and the perioral region [63], this being advantageous in comparison to some commercial membranes (composed of xenogenic collagen) that have demonstrated to do not disrupt the growth of *S. aureus* [64]. Turbidity assays showed that PCL-G-Zn membranes significantly inhibit planktonic bacterial growth compared with the negative control (bacteria in presence of no membranes) and that inhibition was similar for all ZnO-NPs concentrations. This might be due to the release of ZnO-NPs or Zn^{2+} ions in the broth culture media when membranes degradation begins once immersed in the media, which is directly related to the concentration of Zn released from the membranes in the aqueous medium (ICP-MS results). ZnO-NPs

antibacterial effects have been frequently attributed to three mechanisms: 1) mechanical disruption of the cell membrane after contact with NPs [65], 2) destabilization of bacterial membranes by electrostatic interactions with Zn^{2+} ions [28], and 3) oxidative stress by production of reactive oxygen species (ROS) through photocatalysis [28,66]. The third mechanism was not evaluated here since membranes were not incubated under UV radiation; hence, it can be inferred that the antibacterial action observed resulted from the combination of the first two mechanisms due to the membranes released of Zn^{2+} and NPs in the medium. The bacterial cell viability measured by the MTT assay showed that the PCL-G-Zn membranes significantly reduced the biofilm growth on them in comparison to the PCL and PCL-G membranes after 7 days of incubation. This long-term antibacterial effect can be primary assigned to the action of the ZnO-NPs still embedded in the membranes, mainly in the PCL component since the Gel component was dissolved during the first 3 days of incubation. A recent study also reported the antibacterial efficacy of PCL-Gel electrospun membranes but loaded with considerably higher concentrations of ZnO-NPs (5, 15 and 30 w% relative to the total polymer weight) than those in the present study [32]. The use of low antibacterial NPs concentration in GTR membranes is an important finding of the present work, despite NPs are very promising alternative antibacterial agent for medical applications, there are still concerns about the possible long-term side effects of NPs in living beings; thus, it is necessary to limit the concentration of NPs released into the host tissue by using the minimum effective doses [33,67]. Moreover, in future clinical applications, the reduction of the amount of NPs in membranes would reduce their production costs. Currently, there are a few valuable reports of GTR electrospun membranes with NPs-based antibacterial properties such as PCL/Silica-NPs, PCL/ZnO-NPs, PCL/Gel/ZnO-NPs, PCL/polyethyleneglycol (PEG)/bioactive glass

nanopowders (BGs), and PCL-fumarate (PCL-F)/gelatin based with Si and Mg co-doped fluorapatite NPs membranes [32,68–71]. However, the GTR membranes developed in this study seems to be more efficient in terms of the NPs effective-dose, easier to manufacture, and more stable in wet environment than some of those membranes.

On the other hand, the potential toxicity associated with the release products of the membranes may negatively influence the ability of periodontal cells to repopulate and regenerate the defect site, causing further problems. The viability of hFOB and hGF-1 after exposure to lixiviates from the membranes, indicated that PCL-G30-Zn membranes with 1, 3 and 6 w% of ZnO-NPs were biocompatible as they exhibited $\approx 100\%$, $\approx 85\%$ and $\approx 80\%$ of hFOB viability, respectively, in comparison with the positive control; however, in the case of PCL-G45 membranes, only the PCL-G45-1Zn membrane showed more than $\approx 50\%$ of hFOB viability (CV% $\approx 85\%$). The viability of hGF-1 indicated that only PCL-G-Zn membranes with 1 w% of ZnO-NPs were biocompatible as they displayed $\approx 90\%$ of hGF-1 viability, relative to the positive control. From the ICP-MS test measurements, it could be inferred that Zn toxic dose in the medium for the hFOB was between ≈ 35 and ≈ 53 ppm, and for the hGF-1 was between ≈ 7 and ≈ 16 ppm. These results are in agreement with previous reports of ZnO-NPs release effects on eukaryotic cells [58,72], and with the reported Zn-based NPs dosages of median lethal concentration (LC_{50}) for small invertebrates (1.79-67.97 ppm) [73]. Therefore, the present PCL-30G-1Zn and PCL-45G-1Zn membranes are expected to appropriately sustain the viability of periodontal cells around them but significantly inhibit bacterial adhesion and consequently biofilm formation.

5. Conclusion

The PCL-G30 membranes loaded with 1 w% of ZnO-NPs showed the most appropriate physical, chemical and mechanical properties for being used as GTR membranes. Additionally, these membranes prevented planktonic and biofilm growth of *S. aureus* and were simultaneously biocompatible to human osteoblasts (hFOB) and gingival fibroblasts (hGF-1). The present work provides valuable information for the development of biocompatible, biodegradable and mechanically stable membranes with local antibacterial properties that could be used as a promising alternative for improving the clinical success of GTR treatments.

References

[1] THORKILKDA RRING, S TUREN YMANJ AGLA. Development of the biological concept of guided tissue regeneration - animal and human studies. Periodontology 1993;1:26–35.

[2] Academy A. Does periodontal tissue regeneration really work ? 2009;51:208–19.

[3] Ahuja A, Ahuja V, Singh K. Current concepts of regenerative biomaterials in implant dentistry. J Int Clin Dent Res Organ 2016;7:34. doi:10.4103/2231-0754.172943.

[4] Sander L, Karring T. New Attachment and Bone-Formation in Periodontal Defects Following Treatment of Submerged Roots with Guided Tissue Regeneration. J Clin Periodontol 1995;22:295–9.

[5] Giannitelli SM, Basoli F, Mozetic P, Piva P, Bartuli FN, Luciani F, et al. Graded porous polyurethane foam: A potential scaffold for oro-maxillary bone regeneration. Mater Sci Eng C 2015;51:329–35. doi:10.1016/j.msec.2015.03.002.

[6] Cook J. Antibacterial surfaces for biomedical devices 2009;6:553–67.

[7] Bosworth LA, Downes S. Electrospinning for Tissue Regeneration. 2011. doi:10.1533/9780857092915.

[8] Guarino V, Alvarez-Perez M, Cirillo V, Ambrosio L. HMSC interaction with PCL and PCL/gelatin platforms: A comparative study on films and electrospun membranes. J Bioact Compat Polym 2011;26:144–60. doi:10.1177/0883911511399410.

[9] Qian Y, Zhang Z, Zheng L, Song R, Zhao Y. Fabrication and Characterization of Electrospun Polycaprolactone Blended with Chitosan-Gelatin Complex Nanofibrous Mats. J Nanomater 2014;2014:1–7. doi:10.1155/2014/964621.

[10] Gomes SR, Rodrigues G, Martins GG, Roberto MA, Mafra M, Henriques CMR, et al. In vitro and in vivo evaluation of electrospun nanofibers of PCL, chitosan and gelatin: A comparative study. Mater Sci Eng C 2015;46:348–58. doi:10.1016/j.msec.2014.10.051.

[11] Van Doren SR. Matrix metalloproteinase interactions with collagen and elastin. Matrix Biol 2015;44–46:224–31. doi:10.1016/j.matbio.2015.01.005.

[12] Bunyaratavej P, Wang H-L. Collagen Membranes: A Review. J Periodontol 2001;72:215–29. doi:10.1902/jop.2001.72.2.215.

[13] Van Vlierberghe S, Vanderleyden E, Boterberg V, Dubruel P. Gelatin functionalization of biomaterial surfaces: Strategies for immobilization and visualization. Polymers (Basel) 2011;3:114–30. doi:10.3390/polym3010114.

[14] Başaran İ, Oral A. Grafting of poly(ε-caprolactone) on electrospun gelatin nanofiber through surface-initiated ring-opening polymerization. Int J Polym Mater Polym Biomater 2018:1–8. doi:10.1080/00914037.2017.1417287.

[15] Feng B, Duan H, Fu W, Cao Y, Zhang WJ, Zhang Y. Effect of inhomogeneity of the electrospun fibrous scaffolds of gelatin/polycaprolactone hybrid on cell proliferation. J Biomed Mater Res - Part A 2015;103:431–8. doi:10.1002/jbm.a.35184.

[16] Kishan AP, Nezarati RM, Radzicki CM, Renfro AL, Robinson JL, Whitely ME, et al. In situ crosslinking of electrospun gelatin for improved fiber morphology retention and tunable degradation. J Mater Chem B 2015;3:7930–8. doi:10.1039/C5TB00937E.

[17] Papa A, Guarino V, Cirillo V, Oliviero O, Ambrosio L. Optimization of Bicomponent Electrospun Fibers for Therapeutic Use: Post-Treatments to Improve Chemical and Biological Stability. J Funct Biomater 2017;8:47. doi:10.3390/jfb8040047.

[18]   Jiang YC, Jiang L, Huang A, Wang XF, Li Q, Turng LS. Electrospun polycaprolactone/gelatin composites with enhanced cell?matrix interactions as blood vessel endothelial layer scaffolds. Mater Sci Eng C 2017;71:901–8. doi:10.1016/j.msec.2016.10.083.

[19]   He X, Feng B, Huang C, Wang H, Ge Y, Hu R, et al. Electrospun gelatin/polycaprolactone nanofibrous membranes combined with a coculture of bone marrow stromal cells and chondrocytes for cartilage engineering. Int J Nanomedicine 2015;10:2089–99. doi:10.2147/IJN.S79461.

[20]   Fee T, Surianarayanan S, Downs C, Zhou Y, Berry J. Nanofiber alignment regulates NIH3T3 cell orientation and cytoskeletal gene expression on electrospun PCL+gelatin nanofibers. PLoS One 2016;11:1–12. doi:10.1371/journal.pone.0154806.

[21]   Strobel HA, Calamari EL, Beliveau A, Jain A, Rolle MW. Fabrication and characterization of electrospun polycaprolactone and gelatin composite cuffs for tissue engineered blood vessels. J Biomed Mater Res - Part B Appl Biomater 2018;106:817–26. doi:10.1002/jbm.b.33871.

[22]   Xue J, He M, Liu H, Niu Y, Crawford A, Coates PD, et al. Drug loaded homogeneous electrospun PCL/gelatin hybrid nanofiber structures for anti-infective tissue regeneration membranes. Biomaterials 2014;35:9395–405. doi:10.1016/j.biomaterials.2014.07.060.

[23]   Marques MS, Zepon KM, Petronilho FC, Soldi V, Kanis LA. Characterization of membranes based on cellulose acetate butyrate/poly(caprolactone)triol/doxycycline and their potential for guided bone regeneration application. Mater Sci Eng C 2017;76:365–73. doi:10.1016/j.msec.2017.03.095.

[24]   Shi R, Ye J, Li W, Zhang J, Li J, Wu C, et al. Infection-responsive electrospun nanofiber mat for antibacterial guided tissue regeneration membrane. Mater Sci Eng C 2019;100:523–34. doi:10.1016/j.msec.2019.03.039.

[25]   Organization WH. Antimicrobial resistance: global report on surveillance. Who 2014:8. doi:1.4.2014.

[26]   Pati R, Mehta RK, Mohanty S, Padhi A, Sengupta M, Vaseeharan B, et al. Topical application of zinc oxide nanoparticles reduces bacterial skin infection in mice and exhibits antibacterial activity by inducing oxidative stress response and cell membrane disintegration in macrophages. Nanomedicine Nanotechnology, Biol Med 2014;10:1195–208. doi:10.1016/j.nano.2014.02.012.

[27]   Salem W, Leitner DR, Zingl FG, Schratter G, Prassl R, Goessler W, et al. Antibacterial activity of silver and zinc nanoparticles against Vibrio cholerae and enterotoxic Escherichia coli. Int J Med Microbiol 2015;305:85–95. doi:10.1016/j.ijmm.2014.11.005.

[28]   Sarwar S, Chakraborti S, Bera S, Sheikh IA, Hoque KM, Chakrabarti P. The antimicrobial activity of ZnO nanoparticles against Vibrio cholerae: Variation in response depends on biotype. Nanomedicine Nanotechnology, Biol Med 2016;12:1499–509. doi:10.1016/j.nano.2016.02.006.

[29]   He W, Jia H, Cai J, Han X, Zheng Z, Wamer WG, et al. Production of Reactive Oxygen Species and Electrons from Photoexcited ZnO and ZnS Nanoparticles: A Comparative Study for Unraveling their Distinct Photocatalytic Activities. J Phys Chem C 2016;120:3187–95. doi:10.1021/acs.jpcc.5b11456.

[30]   Sultana S, Rafiuddin, Khan MZ, Shahadat M. Development of ZnO and ZrO_2 nanoparticles: Their photocatalytic and bactericidal activity. J Environ Chem Eng

2015;3:886–91. doi:10.1016/j.jece.2015.02.024.

[31] Qiu K, He C, Feng W, Wang W, Zhou X, Yin Z, et al. Doxorubicin-loaded electrospun poly(l-lactic acid)/mesoporous silica nanoparticles composite nanofibers for potential postsurgical cancer treatment. J Mater Chem B 2013;1:4601–11. doi:10.1039/c3tb20636j.

[32] Münchow EA, Albuquerque MTP, Zero B, Kamocki K, Piva E, Gregory RL, et al. Development and characterization of novel ZnO-loaded electrospun membranes for periodontal regeneration. Dent Mater 2015;31:1038–51. doi:10.1016/j.dental.2015.06.004.

[33] Huang YW, Cambre M, Lee HJ. The Toxicity of Nanoparticles Depends on Multiple Molecular and Physicochemical Mechanisms. Int J Mol Sci 2017;18. doi:10.3390/ijms18122702.

[34] Papajani B, Qoku E, Malkaj P, Dilo T. The Study of Phase Compound and the Degree of Crystallinity of Recycled LDPE by X-ray Diffractometer and Optical Microscope 2015;4:2228–32.

[35] Disorder D. X-ray determination of crystallinity and diffuse disorder scattering 1961:1180–5. doi:10.1107/S0365110X61003429.

[36] Taghizadeh A, Favis BD. Carbon nanotubes in blends of polycaprolactone/thermoplastic starch. Carbohydr Polym 2013;98:189–98. doi:10.1016/j.carbpol.2013.05.024.

[37] Shieh Y-T, Yang H-S, Chen H-L, Lin T-L. Nonisothermal crystallization of compatible PCL/PVC blends under supercritical CO2. Polym J 2005;37:932–8. doi:10.1295/polymj.37.932.

[38] Govor E, Oceli V, Slouf M, Šitum A. Characterization of Biodegradable Polycaprolactone Containing Titanium Dioxide Micro and 2014;8:577–81.

[39] Benkaddour A, Jradi K, Robert S, Daneault C. Grafting of Polycaprolactone on Oxidized Nanocelluloses by Click Chemistry. Nanomaterials 2013;3:141–57. doi:10.3390/nano3010141.

[40] Hernández AR, Contreras OC, Acevedo JC, Moreno LGN. Poly(ε-caprolactone) degradation under acidic and alkaline conditions. Am J Polym Sci 2013;3:70–5. doi:10.5923/j.ajps.20130304.02.

[41] Gautam S, Dinda AK, Mishra NC. Fabrication and characterization of PCL/gelatin composite nanofibrous scaffold for tissue engineering applications by electrospinning method. Mater Sci Eng C 2013;33:1228–35. doi:10.1016/j.msec.2012.12.015.

[42] Abdelrazek EM, Hezma AM, El-khodary A, Elzayat AM. Spectroscopic studies and thermal properties of PCL/PMMA biopolymer blend. Egypt J Basic Appl Sci 2016;3:10–5. doi:10.1016/j.ejbas.2015.06.001.

[43] Prado-Prone G, Bazzar M, Focarete ML, García-Macedo JA, Perez-Orive J, Ibarra C, et al. Single-step, acid-based fabrication of homogeneous gelatin-polycaprolactone fibrillar scaffolds intended for skin tissue engineering. Biomed Mater 2020.

[44] Feng B, Tu H, Yuan H, Peng H, Zhang Y. Acetic-acid-mediated miscibility toward electrospinning homogeneous composite nanofibers of GT/PCL. Biomacromolecules 2012;13:3917–25. doi:10.1021/bm3009389.

[45] Zhang Y, Ouyang H, Chwee TL, Ramakrishna S, Huang ZM. Electrospinning of gelatin fibers and gelatin/PCL composite fibrous scaffolds. J Biomed Mater Res - Part B Appl Biomater 2005;72:156–65. doi:10.1002/jbm.b.30128.

[46] Angammana CJ, Jayaram SH. Analysis of the effects of solution conductivity on electrospinning process and fiber morphology. IEEE Trans Ind Appl 2011;47:1109–17.

doi:10.1109/TIA.2011.2127431.

[47]   Prado-prone G, Silva-bermudez P, Almaguer-flores A, García-macedo JA, García VI, Rodil SE, et al. Enhanced antibacterial nanocomposite mats by coaxial electrospinning of polycaprolactone fibers loaded with Zn-based nanoparticles. Nanomedicine Nanotechnology, Biol Med 2018:1–12. doi:10.1016/j.nano.2018.04.005.

[48]   Sanders JE, Lamont SE, Mitchell SB, Malcolm SG. Small fiber diameter fibro-porous meshes: Tissue response sensitivity to fiber spacing. J Biomed Mater Res - Part A 2005;72:335–42. doi:10.1002/jbm.a.30259.

[49]   Scaffaro R, Lopresti F, Botta L, Rigogliuso S, Ghersi G. Melt Processed PCL/PEG Scaffold with Discrete Pore Size Gradient for Selective Cellular Infiltration. Macromol Mater Eng 2016;301:182–90. doi:10.1002/mame.201500289.

[50]   Calciolari E. osteogenic properties of hydrophilic and hydrophobic titanium surfaces : Crosstalk between signalling pathways in in vivo models 2018:598–609. doi:10.1111/jre.12550.

[51]   Ma Z, Mao Z, Gao C. Surface modification and property analysis of biomedical polymers used for tissue engineering 2007;60:137–57. doi:10.1016/j.colsurfb.2007.06.019.

[52]   Acosta EJ. Solid-liquid-liquid wettability and its prediction with surface free energy models. Adv Colloid Interface Sci 2019;264:28–46. doi:10.1016/j.cis.2018.10.003.

[53]   Ding SG, Cheng XQ, Jiang ZX, Bai YP, Shao L. Pore morphology control and hydrophilicity of polyacrylonitrile ultrafiltration membranes 2015;41991:1–9. doi:10.1002/app.41991.

[54]   Bartnikowski M, Dargaville TR, Ivanovski S, Hutmacher DW. Degradation mechanisms of polycaprolactone in the context of chemistry, geometry and environment. Prog Polym Sci 2019;96:1–20. doi:10.1016/j.progpolymsci.2019.05.004.

[55]   Li J, Ma J, Jiang T, Khan F, Wang Y, Chen Y, et al. Combined membrane emulsification with biomimetic mineralization: Designing and constructing novel organic-inorganic hybrid microspheres for enzyme immobilization. Compos Sci Technol 2017;141:56–64. doi:10.1016/j.compscitech.2017.01.008.

[56]   Frazier SD, Srubar W V. Evaporation-based method for preparing gelatin foams with aligned tubular pore structures. Mater Sci Eng C 2016;62:467–73. doi:10.1016/j.msec.2016.01.074.

[57]   Mallakpour S, Nouruzi N. Modification of morphological , mechanical , optical and thermal properties in polycaprolactone-based nanocomposites by the incorporation of diacid-modified ZnO nanoparticles 2016:6400–10.

[58]   Felice B, Alejandra M, Cecilia M, David L, Inés M, Karina M, et al. Controlled degradability of PCL-ZnO nano fi brous sca ff olds for bone tissue engineering and their antibacterial activity. Mater Sci Eng C 2018;93:724–38. doi:10.1016/j.msec.2018.08.009.

[59]   M. Coıc, V. Placet, E. Jacquet CM. Mechanical properties of collagen membranes used in guided bone regeneration: A comparative study of three models. Elsevier Masson SAS 2010:286–90. doi:10.1016/j.stomax.2010.10.006.

[60]   Guarino V, Altobelli R, Cirillo V, Cummaro A, Ambrosio L. Additive electrospraying: A route to process electrospun scaffolds for controlled molecular release. Polym Adv Technol 2015;26:1359–69. doi:10.1002/pat.3588.

[61]   Iglhaut J, Aukhil I, Dm S, Mc J, Progenitor KG. Progenitor cell kinetics during guided tissue regeneration in experimental periodontal wounds I vn 1988.

[62]   Academy A. Utilizing collagen membranes for guided tissue regeneration-based root coverage 2012;59:140–57.

[63]   McCormack MG, Smith AJ, Akram AN, Jackson M, Robertson D, Edwards G. Staphylococcus aureus and the oral cavity: An overlooked source of carriage and infection? Am J Infect Control 2015;43:35–7. doi:10.1016/j.ajic.2014.09.015.

[64]   Slutzkey S, Kozlovsky A, Artzi Z, Matalon S. Collagen barrier membranes may accelerate bacterial growth in vitro: A potential clinical risk to regenerative procedures. Quintessence Int (Berl) 2015;46:43–50. doi:10.3290/j.qi.a32821.

[65]   Guo B-L, Han P, Guo L-C, Cao Y-Q, Li A-D, Kong J-Z, et al. The Antibacterial Activity of Ta-doped ZnO Nanoparticles. Nanoscale Res Lett 2015;10:336. doi:10.1186/s11671-015-1047-4.

[66]   Stankic S, Suman S, Haque F, Vidic J. Pure and multi metal oxide nanoparticles: synthesis, antibacterial and cytotoxic properties. J Nanobiotechnology 2016;14:73. doi:10.1186/s12951-016-0225-6.

[67]   Drahansky M, Paridah M., Moradbak A, Mohamed A., Owolabi F abdulwahab taiwo, Asniza M, et al. Toxicological Risk Assessment of Emerging Nanomaterials: Cytotoxicity, Cellular Uptake, Effects on Biogenesis and Cell Organelle Activity, Acute Toxicity and Biodistribution of Oxide Nanoparticles. IntechOpen 2018:18–33. doi:10.5772/intechopen.71833.

[68]   Nasajpour A, Ansari S, Rinoldi C, Rad AS, Aghaloo T, Shin SR, et al. A Multifunctional Polymeric Periodontal Membrane with Osteogenic and Antibacterial Characteristics. Adv Funct Mater 2018;28:1–8. doi:10.1002/adfm.201703437.

[69]   Castro AGB, Diba M, Kersten M, Jansen JA, van den Beucken JJJP, Yang F. Development of a PCL-silica nanoparticles composite membrane for Guided Bone Regeneration. Mater Sci Eng C 2018;85:154–61. doi:10.1016/j.msec.2017.12.023.

[70]   Soltani Dehnavi S, Mehdikhani M, Rafienia M, Bonakdar S. Preparation and in vitro evaluation of polycaprolactone/PEG/bioactive glass nanopowders nanocomposite membranes for GTR/GBR applications. Mater Sci Eng C 2018;90:236–47. doi:10.1016/j.msec.2018.04.065.

[71]   Ahmadi T, Monshi A, Mortazavi V, Fathi MH, Sharifi S, Kharaziha M, et al. Fabrication and characterization of polycaprolactone fumarate/gelatin-based nanocomposite incorporated with silicon and magnesium co-doped fluorapatite nanoparticles using electrospinning method. Mater Sci Eng C 2020;106. doi:10.1016/j.msec.2019.110172.

[72]   Medina-castillo AL, Osorio R, Andre C, Alaminos M, Toledano M. Bioactive Polymeric Nanoparticles for Periodontal Therapy 2016:1–19. doi:10.1371/journal.pone.0166217.

[73]   Hou J, Wu Y, Li X, Wei B, Li S, Wang X. Toxic effects of different types of zinc oxide nanoparticles on algae, plants, invertebrates, vertebrates and microorganisms. Chemosphere 2018;193:852–60. doi:10.1016/j.chemosphere.2017.11.077.